A 10-kW SOFC Low-Voltage Battery Hybrid Power Conditioning System for Residential Use

Jinhee Lee, Jinsang Jo, Sewan Choi, *Senior Member, IEEE*, and Soo-Bin Han, *Member, IEEE*

***Abstract*—This paper proposes a 10-kW power conditioning system for a 5-kW solid oxide fuel cells (SOFCs) low-voltage battery hybrid power generation that has been developed for participation in the 2003 Future Energy Challenge Competition organized by the U.S. Department of Energy and the IEEE. The objective of the competition was to develop a fuel cell inverter with minimum requirement for cost of $40/kW and efficiency of 90%. The proposed power conditioning system consists of the front-end dc-dc converter, the dc-ac inverter and the bidirectional dc-dc converter. Practical issues such as component rating calculation, high-frequency transformer design, heat sink design, and protection are detailed aiming at the cost and efficiency targets. A low-cost implementation of controllers is discussed along with current-mode control, output voltage regulation with capacitor balancing and an SOC control for battery management. A 10-kW hardware prototype was successfully built and tested in the steady-state as well as in the transient-state. Experimental performances are compared to minimum target requirements of the fuel cell inverter. The cost analysis is done based on the spreadsheets evaluation forms provided in the competition.**

***Index Terms*—Fuel cell inverter, future energy challenge, power conditioning system (PCS), solid oxide fuel cell (SOFC)-battery hybrid.**

I. Introduction

THE FUEL-CELL power-generation system is expected to see increasing use in various applications such as stationary loads, automotive applications, and interfaces with electric utilities due to the several advantages over conventional generation systems. These advantages include: 1) low-environmental pollution; 2) highly efficient power generation; 3) diversity of fuels (natural gas, liquid propane gas, methanol, and naphtha); 4) reusability of exhaust heat; 5) modularity; and 6) faster installation [1].

Fuel cells are generally characterized by the type of electrolyte that they use. Solid oxide fuel cells (SOFCs) have grown in recognition as a viable high-temperature fuel-cell technology. The most striking quality of SOFCs is that the electrolyte is in solid state and is not a liquid electrolyte. The high-operating temperature (up to 1000 °C) allows internal reforming, promotes rapid kinetics with nonprecious materials, and produces high-quality byproduct heat for cogeneration or for use in a bottoming cycle. A number of different fuels can be used from pure hydrogen to methane and carbon monoxide. The major advantage of SOFC lies in its efficiencies, ranging from 55% to 60% [2].

TABLE I
System Specification

Design item	Minimum Target Requirement	
Manufacturing cost	Less than US$40/kW in high volume protection	
Output Power	nominal	5 kW continuous @ DPF 0.7
	overload	10 kW overload for 1 minute @ DPF 0.7 5 kW from fuel cell and 5kW from battery
Energy source	Primary source (SOFC)	29 V nominal, 22~41 V_{dc}, 275A max. from 5kW fuel cell
	Battery	48V nominal, +10% ~ -20%, 500Wh
Output voltage	Split single-phase 120V/240V, 60Hz	
	Voltage regulation	± 6%
	Frequency regulation	± 0.1Hz
	THD	Less than 5%
Acoustic noise	Less than 50dBA @ 1.5 m distance	
Overall efficiency	Higher than 90%	
Protection	Over current, over voltage, short circuit, over temperature, and under voltage	

In general, the basic function of a power conditioning system (PCS) in a fuel-cell generation system is to convert a dc power from the fuel cell to a regulated ac power. The PCS, which basically consists of an inverter, is required to have the following characteristics: 1) allowable wide voltage regulation of fuel cell; 2) controllability of output voltage; 3) available for isolated operation and line parallel operation; 4) fast reactive power dispatch; 5) low-output harmonics; 6) high efficiency; and 7) suitable for high-power systems [3]. Fuel-cell production costs are currently decreasing and have nearly achieved energy costs that are competitive with local utility rates. The inverter cost must also decrease, while at the same time increasing efficiency, reliability, and power-quality levels. The cost reduction of the PCS will enable the fuel-cell system to penetrate rapidly into the utility market.

II. Topology Evaluation

Given the competition specification of the PCS in Table I, two types of power circuit topologies are considered as shown in Fig. 1.

Manuscript received October 27, 2004; revised March 16, 2004. Paper no. TEC-00303-2004.

J. Lee is with the R & D Center, Hyosung Heavy Industries, Seoul 137-850, Korea (e-mail: kinojinhee@paran.com).

J. Jo and S. Choi are with the Seoul National University of Technology, Seoul 139-743, Korea (e-mail: jeue@snut.ac.kr; schoi@snut.ac.kr).

S. B. Han is with the Electric Energy and Lighting Research Center, Korea Institute of Energy Research, Daejeon 305-343, Korea (e-mail: sbhan@kier.re.kr).

Digital Object Identifier 10.1109/TEC.2005.858060

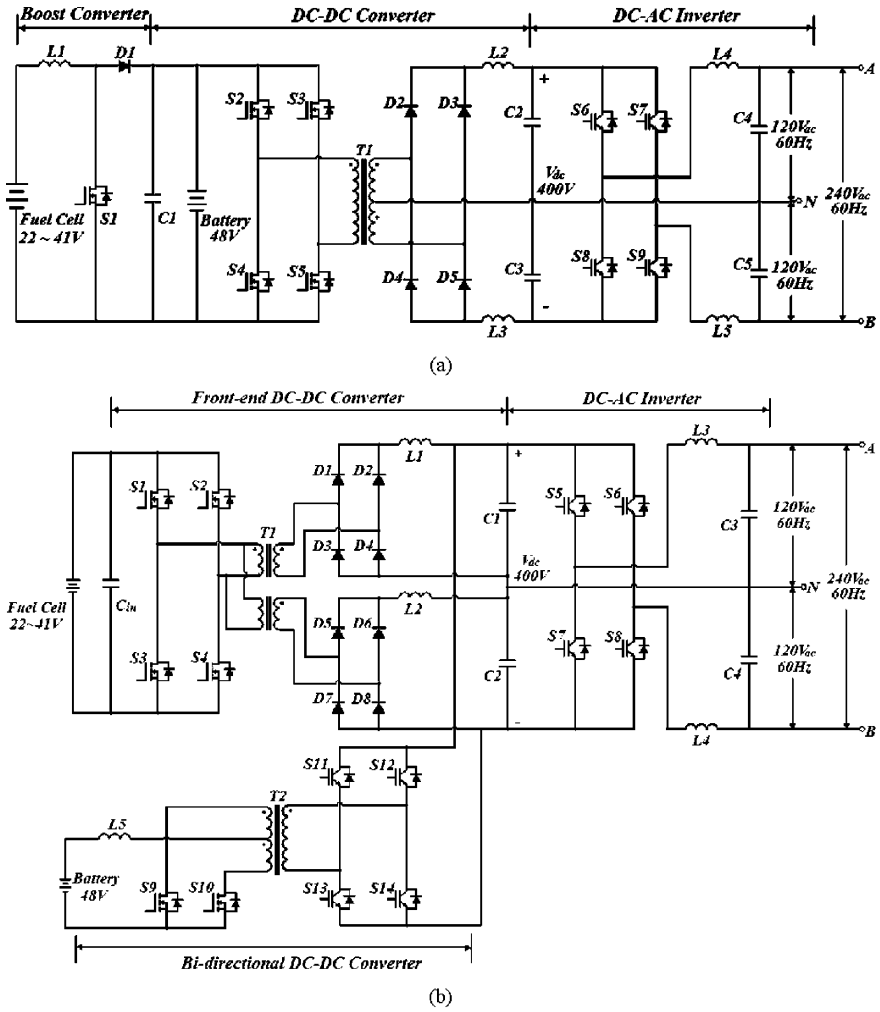

Fig. 1. Two topologies for fuel cell-battery hybrid system. (a) Scheme I (b) Scheme II (Proposed scheme).

In Scheme I, a dc voltage from the fuel-cell output is first boosted to 48 V via a nonisolated boost converter. The 48-V battery bank in the fuel-cell system is connected to the 48-V link so that power flow to and from the battery is controlled by the boost converter. The 48 V_{dc} from the boost converter is then converted to 400 V_{dc} via an isolated high-frequency dc-dc converter. The high-frequency dc-dc converter could be push-pull or full-bridge types. The full-bridge type is preferred especially in this high power step-up application because the high frequency transformer in the push-pull type has a center-tap in the primary winding, and low-voltage, high-current termination is problematic. Furthermore, unequal effective turns may cause switch current unbalance resulting in core saturation. The 400-V dc-dc converter output is then converted to 120 V/240 V, 50/60 Hz, single-phase ac by means of a pulsewidth modulator (PWM) inverter stage.

In Scheme II, a voltage from the fuel-cell output is first converted to 400 V_{dc} via an isolated high-frequency dc-dc converter. In the same way, the 400-V dc-dc converter output is then converted to 120 V/240 V, 50/60 Hz, single-phase ac by means of a PWM inverter stage. The 48-V battery bank is connected to the 400-V dc link via a bidirectional dc-dc converter for charge and discharge modes of operation. A current-source push-pull type at the low-voltage battery side and a voltage-source full-bridge type at the high-voltage dc-link side were chosen, respectively.

Both of the schemes are evaluated from efficiency and cost standpoint.

All the power components of the two schemes are designed for the given system specification and actual devices are selected from some manufactures and listed in Appendix A. Appropriate safety margins were considered for actual device selection. From the datasheet of the selected devices, the power loss is calculated considering the switching and conduction losses for power switching devices, the core and copper losses for magnetic devices, and the ESR loss for capacitors. The loss in the boost switch and diode of the nonisolated boost converter of Scheme I is significant, which exceeds 50% of the total loss. The estimated efficiencies at 5 kW loading are 85.7% for Scheme I and 94.6% for Scheme II, respectively.

Next, cost evaluation is performed based on the spreadsheet, shown in Appendix B, provided by 2003 FEC organizing committee. Cost factors in the spreadsheet are obtained based on the designed value without safety margin. The power switching devices, the transformers, and the capacitors employed in both schemes did not give much difference in cost. However, the cost of the boost inductor in Scheme I is significant due to its high

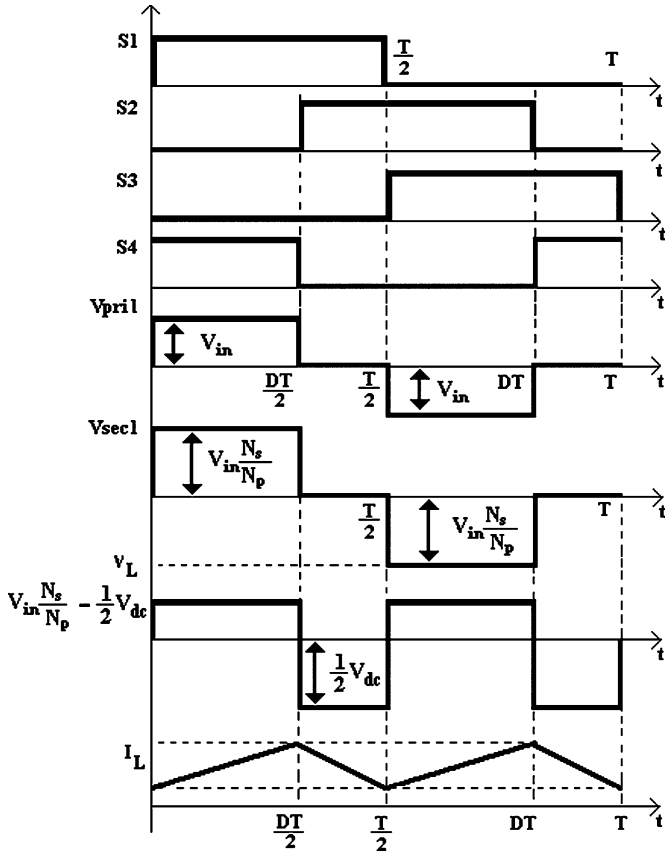

Fig. 2. Main waveforms of the front-end converter.

current capacity (272.5 A). The estimated costs at high volume are \$63.7/kW for Scheme I and \$45.2/kW for Scheme II, respectively. The values in the table indicate only preliminary and relative cost estimates, not dollars. It can therefore be concluded that Scheme II is superior to Scheme I from both efficiency and cost standpoint. Finally, Scheme II is chosen as a power circuit topology for SNUT fuel cell PCS.

III. Proposed Power Conditioning System (PCS)

A. Front-End DC-DC Converter

A front-end dc-dc converter is required to boost an unregulated fuel cell voltage of 29 V nominal to a regulated 400 V. As shown in Fig. 1(b), the full-bridge type with two diode bridges connected in series at the secondary is a topology of choice. High-frequency transformers are employed to allow a low voltage to be boosted to two split 200 V_{dc} buses for the dc link to the inverter. The reason why two 2.5 kW high-frequency transformers are employed instead of a 5-kW high-frequency transformer is that in general leakage inductance could be lower for lower power level. The reduced leakage inductance results in reduced duty loss, and therefore, turns ratio of the transformer is also reduced. This in turn reduces the voltage rating of diodes in the secondary side and the current rating of MOSFETs in the primary side. The "voltage-source" full bridge has been chosen because the inductor in the current source type should have a large peak current rating of 275A, which is too bulky.

Fig. 2 shows the main waveforms of the front-end dc-dc converter. From the inductor voltage V_L an equation can be written as

$$\left(V_{\rm in}\cdot\frac{N_s}{N_p}-\frac{1}{2}\cdot V_{\rm dc}\right)\cdot\frac{DT}{2}=\frac{1}{2}\cdot V_{\rm dc}\cdot\left\{\frac{T\cdot(1-D)}{2}\right\}. \tag{1}$$

Therefore, the duty cycle of the proposed front-end converter is obtained by

$$D=\frac{N_p\cdot V_{\rm dc}}{4\cdot N_s\cdot V_{\rm in}}. \tag{2}$$

According to (2), the duty cycle ranges from 0.24–0.45 to regulate the dc-link voltage of 400 V when the fuel-cell voltage varies between 22 and 41 V.

Fig. 3 shows the block diagram for feedback control of the front-end dc-dc converter. The first goal of the control is to regulate the dc-link voltage. A PI compensator is used for the voltage control. A current control is also implemented to improve the dynamic characteristic of the system and to reduce current ratings of the power components during load transient. The current reference is restricted by a current limiter whose value is adjusted by a command from the fuel-cell controller so that the power drawn from the fuel cell does not exceed its capability. A low-cost phase-shift PWM controller, UC3895, is employed for control of the front-end dc-dc converter. It allows constant frequency PWM in conjunction with resonant zero-voltage switching to provide high efficiency at high frequency [9].

B. DC-AC Inverter

The inverter system consists of two half-bridge inverters, utilizing center tapped link capacitors to generate a split single-phase 120/240 V_{ac}, 60 Hz output as shown in Fig. 1(b). An output $L-C$ filter stage is employed to reduce the ripple component and to draw a low-THD ac-voltage waveform.

A low-cost DSP, Texas Instrument TMS320LF2407, is implemented to provide the control for the inverter system.

The DSP control will offer increased flexibility and will minimize component cost. The goal of the DSP control is as follows: 1) supervise the whole PCS; 2) generate the PWM gating signals for IGBTs in the inverter stage; 3) implement output voltage regulation under varying load conditions; 4) send the bidirectional dc-dc converter a current reference; and 5) communicate with the fuel-cell controller.

To meet the output voltage tolerance requirement the ac output voltage is sensed and a closed-loop control is implemented with a digital PI compensator in the DSP. In the meanwhile, unbalance in dc-link capacitor voltages causes generation of even harmonics in the inverter output voltages. A simple output voltage regulation method with capacitor voltage balancing function is implemented as shown in Fig. 4. Suppose output voltage V_a has a positive dc offset, which means that the upper capacitor voltage is greater than the lower capacitor voltage. The output voltage V_a is sensed and passed through a low-pass filter to obtain a dc component of voltage V_a. This causes addition of a positive value to the reference output voltage V_b^* resulting in

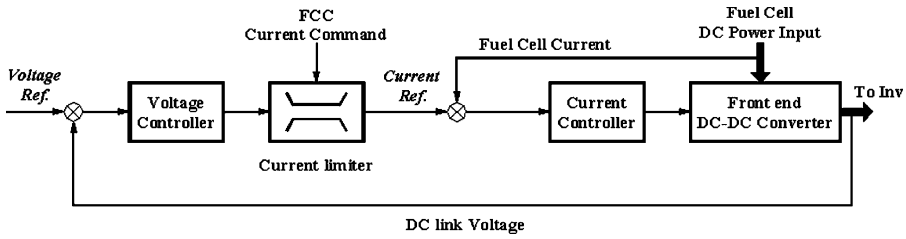

Fig. 3. Control block diagram for the front-end dc-dc converter.

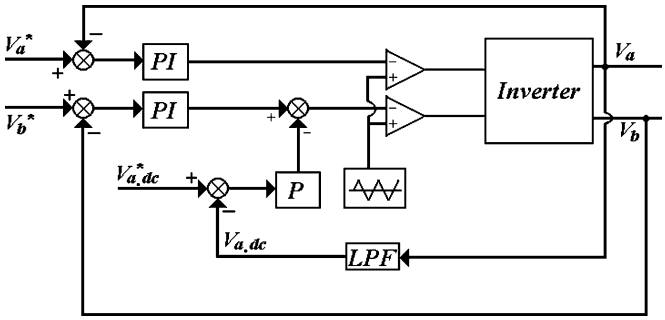

Fig. 4. Output voltage regulation and capacitor voltage balancing.

a decrease in upper capacitor voltage and an increase in lower capacitor voltage.

C. Bidirectional DC-DC Converter

The fuel cell has a slow response, and therefore the power demand from the load and the power supply from the fuel cell does not coincide during a transient dc load. Therefore, a secondary energy source is required to match the power difference between the fuel cell and the load. High voltage batteries could be directly connected to the 400-V dc link without any intermediate power converter, but the high voltage battery is relatively expensive and may have the battery cell unbalance problem in the long run. A 48-V lead acid battery pack is connected to the 400 V dc link via a bidirectional dc-dc converter shown in Fig. 1(b). A current-source push-pull converter employing MOSFETs is operated to discharge the battery whereas a voltage-source full-bridge converter employing IGBTs is operated to charge the battery. The control block diagram for the bidirectional dc-dc converter is shown in Fig. 5. The DSP determines the current reference for the bidirectional dc-dc converter by calculating the difference in real power between the PCS input and the load. The two PWM controllers, UC3825 and UC3895, are employed for charge and discharge modes of operation, respectively. One should be in idle state while the other is in operation. Fig. 6 shows the inductor voltage and current waveforms for charge and discharge modes, respectively. Let us define turns ratio n_2 of the high-frequency transformer T_2 to be

$$n_2 = \frac{N_s}{N_p}. \tag{3}$$

During the charge mode, we have

$$-\left(V_{\rm batt} - \frac{V_{\rm dc}}{n_2}\right) \cdot DT_S = V_{\rm batt} \cdot \left(\frac{1}{2} - D\right) T_S \tag{4}$$

which gives

$$\text{therefore } \frac{V_{\rm batt}}{V_{\rm dc}} = \frac{2D}{n_2} \quad (\text{where}, 0 < D < 0.5). \tag{5}$$

During the discharge mode, we have

$$V_{\rm batt} \cdot D_d T_S = -\left(V_{\rm batt} - \frac{V_{\rm dc}}{n_2}\right) \cdot \left(\frac{1}{2} - D_d\right) T_S \tag{6}$$

which gives

$$\text{therefore } \frac{V_{\rm dc}}{V_{\rm batt}} = \frac{n_2}{(1-2D_d)} \quad (0 < D_d < 0.5) \tag{7}$$

$$\text{therefore } \frac{V_{\rm dc}}{V_{\rm batt}} = \frac{n_2}{2(1-D)} \quad (0.5 < D < 1, \text{where } D = 0.5 + D_d). \tag{8}$$

D. Battery Management

An optimum use of battery combined with fuel cell can reduce the overall cost of the fuel-cell system, or improve the system performance such as reliability and lifetime. To cope with the slow dynamic response of the fuel cell (Maximum Slew Rate = 200 W/min), a 48-V battery pack is used as a secondary energy source to supply transient load since the fuel cell system including a reformer is sluggish even if the fuel cell stack has a fast response.

During an overload condition the PCS is supposed to draw 5 kW from the fuel cell and 5 kW from the battery for maximum 1 minute. Charging and charge management must be provided such that state of charge (SOC) is unchanged at the end of a 24-h test sequence [8]. The proposed PCS determines the mode of operation based on battery SOC. The SOC could be measured simply by integrating the battery charging current $I_{\rm bat}$ as follows:

$$\text{SOC} = \frac{Q_0 - \int i_{\rm bat} dt}{Q_n} \tag{9}$$

where Q_o is initial charge and Q_n is rated ampere-hour of battery. The initial charge Q_o is set to be Q_n when the system starts from full battery charge. More accurate measurement requires in-depth considerations of various parameters such as temperature, discharge rate, age, and cumulative calculation errors [5], [6]. But this research is out of paper's scope and it is the authors' intention to show the mode of operation determined by SOC as an index.

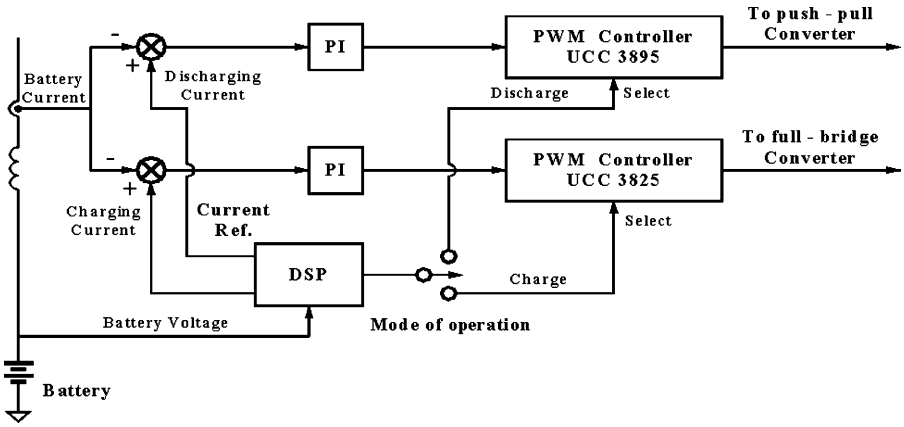

Fig. 5. Control block diagram for the bidirectional dc-dc converter.

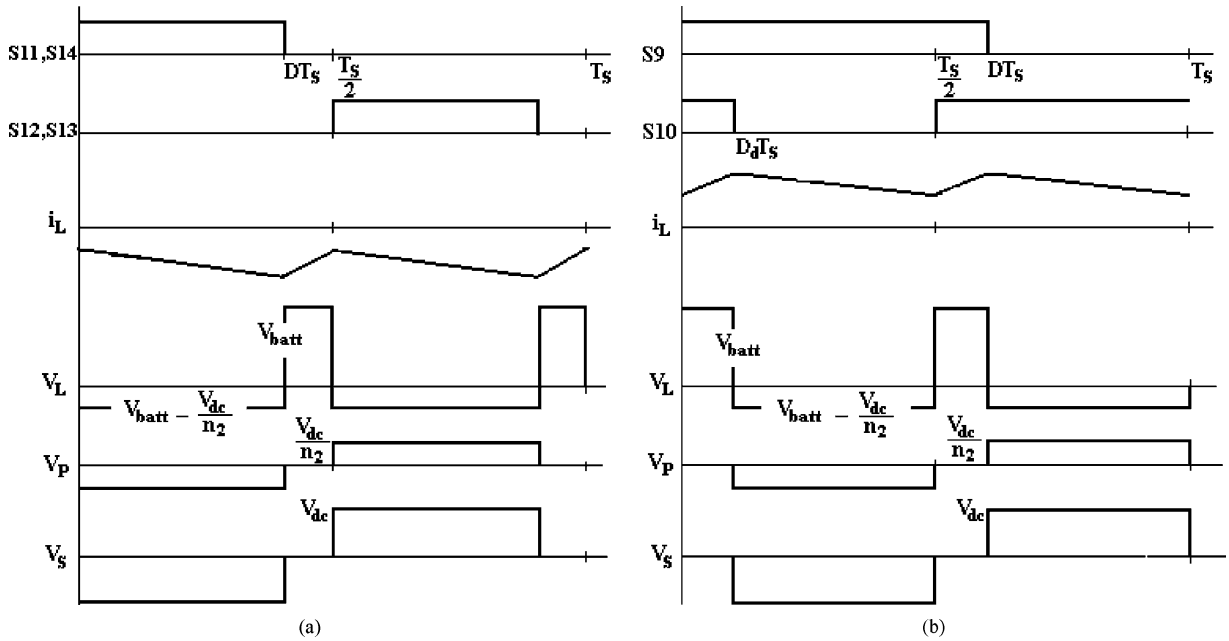

Fig. 6. Inductor voltage & current waveforms (a) Charge mode (b) Discharge mode.

In hybrid electric vehicle system, for example, where regeneration braking is considered the SOC is maintained between 0.4 and 0.8. However, in general, the SOC is controlled to be maintained at 1 for residential use, which is also the specification of the competition. Detailed operational procedure is as follows. When the load power exceeds 5 kW, which is the maximum output power of the fuel cell, the battery starts to discharge through a bidirection converter and keeps the discharge operation until the overload condition is removed. When the load jumps, but not overloaded, the battery should also discharge until the fuel-cell power increases and matches the demanded load power. After the discharging mode ends, the fuel-cell power continues to increase to charge the battery as far as the SOC is lower than 1 and keeps the charge operation and until the SOC reaches 1. During the charge mode, the fuel-cell charges the battery with a current proportional to depth of discharge, but limits the charge current to a maximum value recommended by manufacturer. The magnitude of the charging current for the proposed fuel-cell system is determined as shown in Fig. 7.

E. Protection and Diagnostic

The proposed PCS provides the protection capabilities of over current, short circuit, over/under voltage and over temperature in the circuit. Table II lists all the protection functions which have been implemented in the proposed PCS. The PWM control IC such as UC3895 provides the capability to detect any fault signal through an input pin of the chip and will shut down the chip by disabling all the gate signals to the switches.

Temperature protection is implemented by using a bimetal as a temperature sensor that is mounted on the heat sink. If the temperature of the sensor rises over 60 °C a fan on the heat sink starts to operate. If the temperature of the sensor rises over 80 °C a signal is sent to the gate drive for immediate shutdown. A computer is connected to the inverter system so that various system

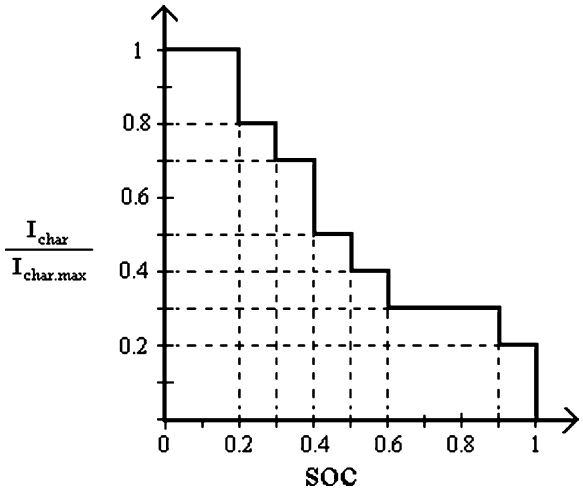

Fig. 7. Battery charging current.

TABLE II
PROTECTION

Fuel Cell	OV (over 41V), UV (under 22V), OC (over 275A)
dc-link	OV (over 500V), UV (under 300V)
Load	OC (100%~110%, 1min.), SC (over 110%)
Battery	OV (over 56.7V), UV (under 42V)
Heatsink	Over 60°C → Fan Start, Over 80°C → Shutdown

parameters such as output phase voltage, output phase current, output power, frequency of the output voltage and some inverter status including alarms and faults could be monitored. All the data monitored are also recorded in the computer and updated every two minutes so that inverter status could be interpreted after the fault has occurred.

IV. Power Component Design

The power components of the proposed PCS are designed with the following system parameter:

- switching frequency of the front-end dc-dc converter: 25 kHz;
- switching frequency of the dc-ac converter: 20 kHz;
- switching frequency of the bidirectional dc-dc converter: 20 kHz;
- dc-link voltage V : 400 V;
- transformer turns ratio $N_{p1} : N_{s1} = 1 : 10$;
- permissible ripple current $\Delta I_{L1} = 50\%$ of maximum dc-link current.
- permissible ripple voltage $\Delta V_{c1} = 10\%$ of dc-link voltage.

1) Power Switches: The ratings of the power switching devices used in each converter part are listed in Appendix A. A safety margin for MOSFETs and diodes in the front-end dc-dc converter should be considered due to voltage spikes originated from the leakage inductance and/or the ringing phenomenon at the secondary winding of the high-frequency transformer. An ultrafast recovery diode is chosen to lower the switching loss due to the high-switching frequency operation. Since the maximum battery discharge current is much larger than the maximum battery charge current, the switch ratings of the bidirectional dc-dc converter should also be determined based on the discharge mode of operation at full load (5 kW, 1 min).

2) High-Frequency Transformer: Ferrite core is chosen as a material of a high-frequency transformer. The power handling capacity of a transformer core can be determined by its area product $\boldsymbol{W}_a \boldsymbol{A}_c$, where $\boldsymbol{W}_a$ is the available core window area, and $\boldsymbol{A}_c$ is the effective core cross-sectional area.

The area product $\boldsymbol{W}_a \boldsymbol{A}_c$ is given by [10]

$$W_a A_c = \frac{P_{\rm dc} \cdot C \cdot 10^8}{4 \cdot e \cdot B \cdot f_s \cdot K} = 23.47 \text{ cm}^4 \tag{10}$$

where $\boldsymbol{P}$ is output power, $\boldsymbol{C}$ is current capacity which is 5.07×10^{-3} cm^2/Amp for "**EER**" core, $\boldsymbol{e}$ is transformer efficiency which is assumed to be 90%, $\boldsymbol{B}$ is flux density that is assumed be 2000 (Gauss), $\boldsymbol{f}_s$ is switching frequency and $\boldsymbol{K}$ is winding factor which is 0.3 for primary side only. Using the core selection table by area product distribution, the core of 47054-EC was selected. Once a core is chosen, the calculation of primary and secondary turns and their wire sizes is readily accomplished. The number of primary turns is given by [10]

$$N_p = \frac{V_P \cdot 10^8}{4 \cdot B \cdot A \cdot f_s} = \frac{41 \cdot 10^8}{4 \cdot 2000 \cdot 3.39 \cdot 25000} = 3.18 \text{ turns} \tag{11}$$

Here, $\boldsymbol{V}_p$ is peak primary voltage and $\boldsymbol{A}$ is cross-sectional area of the core. Considering duty loss of 20% which is originated from the leakage inductance at the secondary winding of the transformer, the final number of turns for primary and secondary windings is determined to be $N_p : N_s = 6 : 90$. The wire sizes AWG 0 and AWG 12 are selected from AWG table for the primary and secondary wires whose circular mil requirements are 93 500 and 5 900, respectively. Ritz wires were used to reduce the copper loss due to skin effect.

3) DC-Link Inductor and Capacitors: From (1), the inductance can be obtained by

$$L = \frac{(1-2D) \cdot \left(\frac{N_s}{N_p}\right) \cdot V_{\rm in} \cdot D}{\Delta I \cdot f_s} = 100 \ \mu\text{H}. \tag{12}$$

At displacement factor of 0.7 the maximum output VA becomes

$$\text{VA}_{\rm out} = \frac{10000}{0.7} = 14280 \text{ VA}. \tag{13}$$

The full load current per phase is given by

$$I_{a,\rm rms} = \frac{14280}{2 \cdot 120} = 59.5 \text{ A}. \tag{14}$$

For the sake of simplicity, the output current i_a is assumed to consist of only fundamental $(I_{a,1})$ and third harmonic $(I_{a,3})$ components. Further, assuming $I_{a,3} = 0.7 I_{a,1}$ since this is a typical case of a single-phase rectifier type nonlinear load [4],

$$I_{a\cdot\rm rms} \cong \sqrt{I_{a,1}^2 + I_{a,3}^2} = 1.22 I_{a,1}. \tag{15}$$

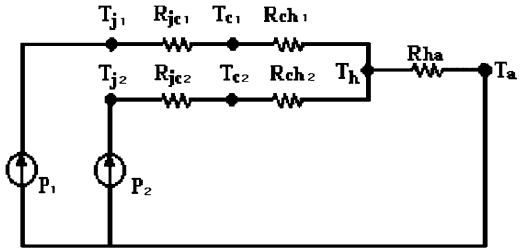

Fig. 8. Thermal equivalent circuit.

The most dominant component of the dc-link capacitor current i_{c1} is the fundamental frequency current, the rms value of which equals

$$I_{c1,1} \cong \frac{1}{2} \cdot I_{a,1} = 24.3 \text{ A}. \tag{16}$$

Capacitance can be obtained by

$$C_1 = \frac{I_{c1,1}}{\omega \Delta V_{c1}} = \frac{24.3}{2\pi \cdot 60 \cdot 20} = 3222 \ \mu\text{F}. \tag{17}$$

4) Output Filter: Based on the design procedure in [4], the filter inductance and capacitance become

$$L_f = \frac{X_L}{2\pi f_1} = \frac{0.035}{2\pi \cdot 60} = 92.84 \ \mu\text{H} \tag{18}$$

$$C_f = \frac{1}{2\pi \cdot f_1 \cdot X_c} = 16 \ \mu\text{F}. \tag{19}$$

5) Battery Inductor: The ripple component in the charging current should be restricted by an inductor on the battery side. The magnitude of the charging current depends on the capacity of the battery. The maximum charging current is assumed to be 45A for battery of 48 V, 155 Ah. We allow the ripple current to be 20% of the maximum charging current, that is, $\Delta i_L = 9$ A.

During the charge mode, the duty ratio D lies between $0.33 < D < 0.5$.

When the switches S11 and S14 are turned on during the charge mode we have (see Fig. 6)

$$\frac{(V_{\text{dc}}/n_2) - V_{\text{batt}}}{L} = \frac{\Delta i_L}{DT_S}. \tag{20}$$

Then, the worst case inductance is obtained by

$$\text{therefore } L = \frac{(1-2D) \cdot D}{n_2 \cdot \Delta i_L \cdot f_s} \cdot V_{\text{dc}} = 39 \ \mu\text{H}. \tag{21}$$

The current rating of the inductor is dominated by discharge mode of operation. The rms inductor current at a maximum discharge becomes $I_L = 113$ (A).

6) Heat Sink: The heat sink is a crucial and a costly component of the PCS. The first step is to calculate the power dissipation of switching devices. Then, a thermal equivalent circuit for analyzing thermal characteristic of the heat sink is defined as shown in Fig. 8, where two different power devices are mounted on a heat sink. Given power loss P_l (where $l = 1$ or 2) of a switching device, junction to case thermal resistance $R_{jc,l}$, case to heat sink thermal resistance $R_{ch,l} = 0.3$°C/W, ambient temperature $T_a = 40$ °C, and juntion temperature $T_{j,l}$, heat sink to ambient thermal resistance R_{ha} can be obtained in the following procedure. The case temperature $T_{c,l}$ can be given as:

$$T_{c,l} = T_{j,l} - P_l \cdot R_{jc,l}. \tag{22}$$

Then, heat sink temperature $T_{h,l}$ can be given as

$$T_{h,l} = T_{c,l} - P_l \cdot R_{ch,l}. \tag{23}$$

Then, the total heat sink temperature T_h is

$$T_h = T_{h,1} + T_{h,2}. \tag{24}$$

Finally, heat sink to ambient thermal resistance R_{ha} is obtained by

$$R_{ha} = \frac{T_h - T_a}{P_1 + P_2}. \tag{25}$$

Table III summarizes the thermal calculation required for the heat sink design. Using the heat sink to ambient thermal resistance, the required area of the heat sink can be calculated or the heat sink can directly be selected from a manufacture by the heat sink to ambient thermal resistance obtained.

TABLE III
THERMAL CHARACTERISTICS FOR THE HEAT SINK DESIGN

Section	Device	Power loss per unit (W)	R_{jc} (°C/W)	T_j (°C)	T_c (°C)	T_h (°C)	R_{ha} (°C/W)
Front-end dc–dc	MOSFET	48.9	0.21	70.26	60	45.4	0.11
	Diode	13.2	1.25	65.85	49.3		
Inverter	IGBT	120.9	0.22	112.5	85.9	49.7	0.08
Bi -directional dc–dc	MOSFET	107.7	0.18	103.3	80.9		
	IGBT	39.9	0.31	67.5	55.2		

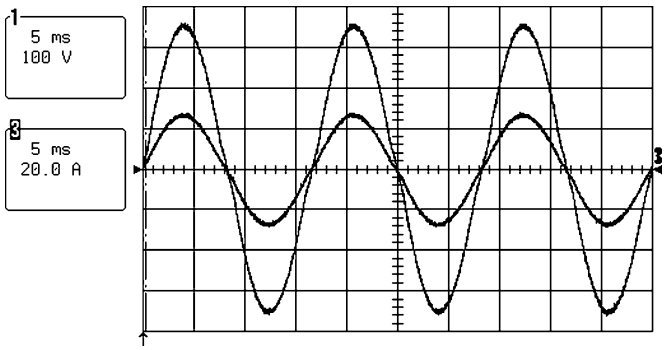

Fig. 9. Experimental waveforms (4.4 kW load): output voltage and current : phase AB.

V. EXPERIMENTS AND PERFORMANCE EVALUATION

The steady-state output voltage and current waveforms at a 4.4-kW load level are shown in Fig. 9. The experimental waveforms were also obtained at a discharge mode of operation, that is, at a load increase from 2–2.7 kW. In this experiment a dc power supply emulates the fuel cell. The lower trace in Fig. 10(a) shows an increase of the output phase current, and the upper trace in Fig. 10(a) shows the output phase voltage that is well regulated during the load increase. The upper trace in Fig. 10(b)

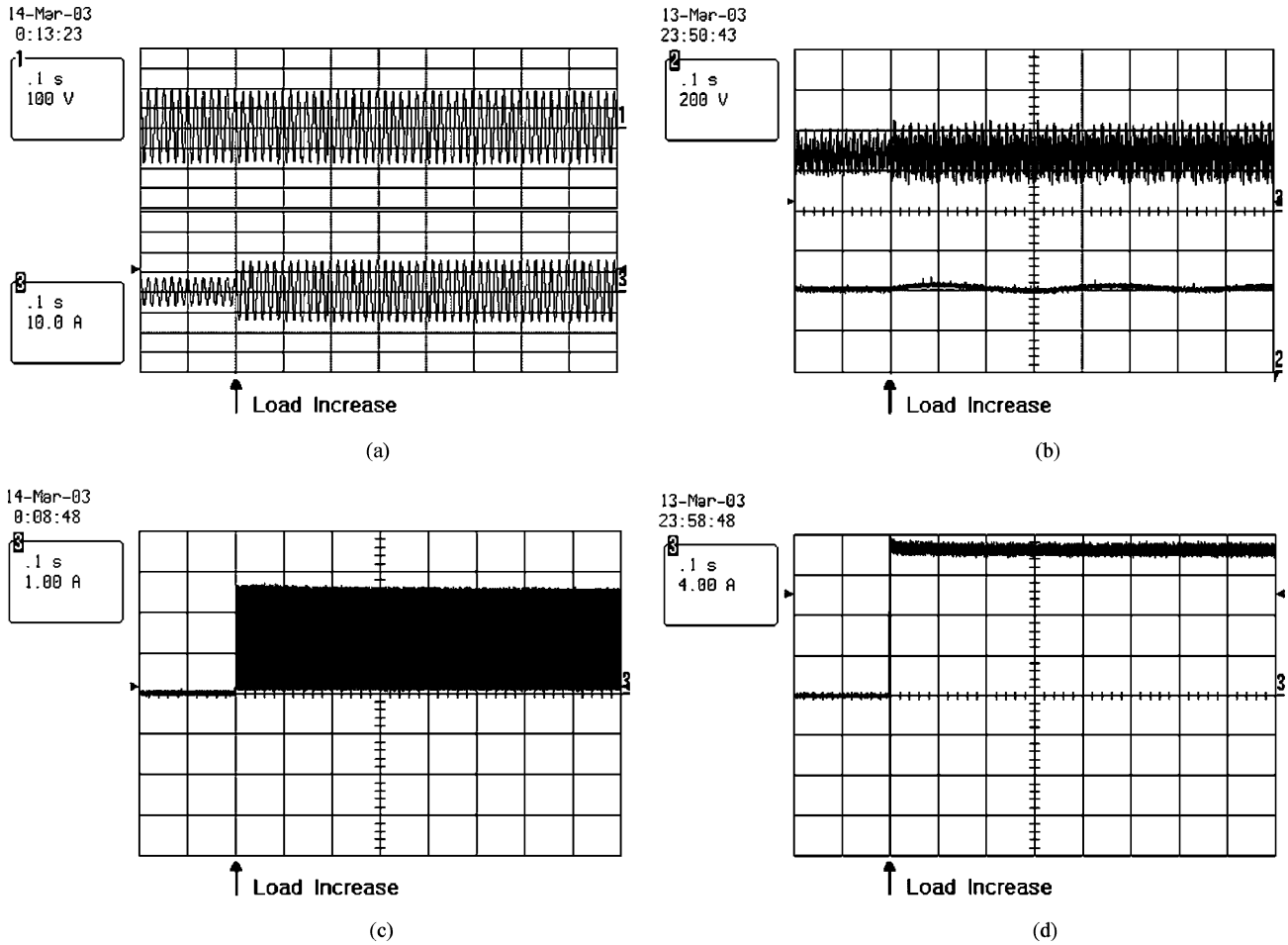

Fig. 10. Experimental waveforms (2 → 2.7 kW). (a) Output phase voltage and current, (b) upper: output current of the front-end converter; lower: dc-link voltage, (c) output current of the bidirectional converter, and (d) battery current.

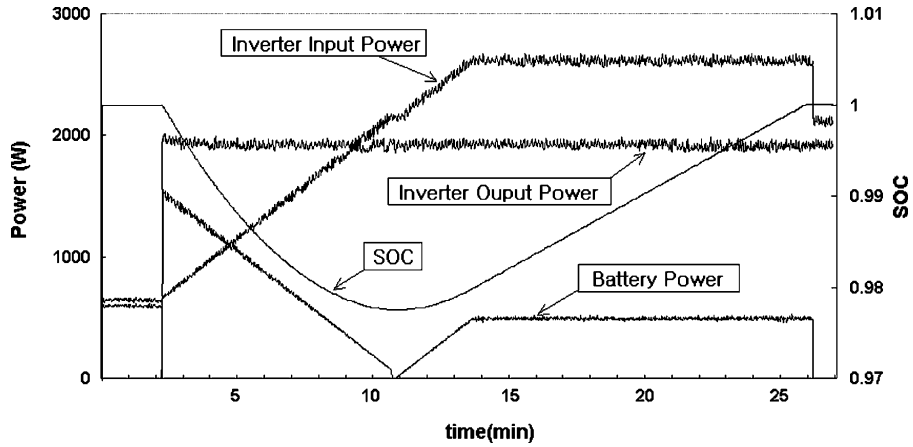

Fig. 11. SOC control for battery management.

shows the output current of the front-end dc-dc converter whose average value did not change after the transient even if the ripple was slightly increased due to operation of bidirectional dc-dc converter. The lower trace in Fig. 10(b) shows the dc-link voltage, which undergoes a slight overshoot and is stabilized. Fig. 10(c) shows the PWM current waveform on the dc-link side of the bidirectional dc-dc converter. Fig. 10(d) shows the current waveform on the battery side of the bidirectional dc-dc. This demonstrates that at a sudden load increase the output voltage is well regulated while the bidirectional dc-dc converter would quickly draw the power difference from battery. Fig. 11 shows variations in SOC and in real power of the PCS input, load and battery sides. Initially, the fuel cell is supplying a load of 600 W, and the SOC is being kept at 1. The load power

Fig. 12. Photograph of the SNUT fuel-cell inverter.

TABLE IV
EXPERIMENTAL PERFORMANCE (NO LOAD TO 4.4 kW LOAD)

Design Item	2003 FEC Specification performance	SNUT team Experimental performance
Frequency	60Hz ±0.1Hz	59.95 Hz ~ 60.09 Hz
THD (Output voltage harmonic)	5%	Lower than 1.94%
Regulation	±6%	-2.4% ~ +0.2%
Input current ripple	3%	Lower than 2.2%
Efficiency	Higher than 90%	Total 88% at 4.4 kW load (dcdc:90%, INV:97%)
Cost	$40/kW	$45.18/kW

jumps to 2000 W = 2.13 min, and the battery immediately starts to discharge with a current corresponding to the power difference. The SOC starts to decrease from this moment. As the PCS input power increases at a rate of 200 W/min, the battery power decreases at the same rate until it reaches the demanded load power plus losses. Since the SOC is supposed to be maintained at 1 in this system, the PCS input power continues increasing to charge the battery until a charging current is set up. The PCS keeps charging with the constant charging current and finishes the battery charge mode when the SOC reaches 1. Photograph of the SNUT fuel-cell inverter system is shown in Fig. 12. Experimental performances of some important design items have been obtained and listed in Table IV. As shown in Table IV, the SNUT fuel-cell inverter met the minimum target requirements for most of the design items such as frequency regulation, THD of the output voltage, output voltage regulation and input current ripple.

VI. CONCLUSION

In this paper, a 10-kW power conditioning system for 5-kW SOFC low-voltage battery hybrid power generation has been proposed for the 2003 Future Energy Challenge Competition, which is organized by the U.S. Department of Energy and IEEE. The objective of the competition was to develop a fuel-cell inverter with minimum requirement for cost of $40/kW and efficiency of 90%. Many practical issues such as component rating calculation, high frequency transformer design, heat sink design, and protection have been detailed. Battery management has been performed by a SOC control. The SNUT prototype inverter met the minimum target requirements and demonstrated a good performance in most of the design items.

APPENDIX A

TABLE V
POWER LOSS ESTIMATION (AT 5 kW, SCHEME I)

Section	Component	Actual device Selection	Loss(W)	
Non -isolated Boost	MOSFET (S1)	APT10M07JVR (100V, 225A, 7mΩ)	$P_{cond.}$	122.1
			$P_{sw.}$	40.7
	Diode (D1)	DSEI2x161-12P (1200V, 2X128A, trr = 35ns)	$P_{cond.}$	335.6
			$P_{sw.}$	0.9
	Inductor (L1)	MAGNETICS 43208 (EI)	P_{copper}	7.77
	Capacitor (C1)	Samwha, SZ2A338M35100 (100V, 3300uF, ESR 0.08Ω)	P_{ESR}	29.2
Isolated dc-dc	MOSFET (S2~S5)	IXFN340N07 (70V, 340A, 4mΩ)	$P_{cond.}$	63.3
			$P_{sw.}$	29.8
	Trans. (T1)	MAGNETICS 49925 (U)	P_{core}	31.9
			P_{copper}	45.8
	Diode (D2 ~ D9)	DESI 30-10A (1000V, 30A, trr = 50ns)	$P_{cond.}$	20.6
			$P_{sw.}$	0.03
	Inductor (L2, L3)	Chang-sung CH270125E (Toroid)	P_{copper}	0.15
	Capacitor (C2, C3)	Samwha, GF2G688M76160 (400V, 6800uF, ESR 0.04Ω)	P_{ESR}	0.15
Inverter	IGBT (S6~S9)	MG50Q2YS50 (600V, 50A, $V_{CE(sat)}$ 2.7V)	$P_{cond.}$	36.7
			$P_{sw.}$	29.4
	Inductor (L4, L5)	Chang-sung CH572060E (Toroid)	P_{core}	1.65
			P_{copper}	0.007
	Capacitor (C4, C5)	Digital Tech (250V, 15uF, ESR 0.04Ω)	P_{ESR}	69.2
Total Loss			864.9	

TABLE VI
POWER LOSS ESTIMATION (AT 5 kW, SCHEME II)

Section	Component	Actual device Selection	Loss(W)	
Front-end dc-dc	MOSFET (S1~S4)	IXFN340N07 (70V, 340A, 4mΩ)	$P_{cond.}$	63.3
			$P_{sw.}$	29.8
	Trans. (T1)	MAGNETICS 49925 (U)	P_{core}	15.9
			P_{copper}	24.9
	Diode (D1~D8)	DESI 30-10A (1000V, 30A, trr=50ns)	$P_{cond.}$	13.2
			$P_{sw.}$	0.01
	Inductor (L1, L2)	Chang-sung CH270125E (Toroid)	P_{copper}	0.07
	Capacitor (C1, C2)	Samwha, SZ2A338M35100 (100V, 3300uF, ESR 0.08Ω)	P_{ESR}	0.004
Inverter	IGBT (S5~S8)	MG50Q2YS50 (600V, 50A, , $V_{CE(sat)}$ 2.7V)	$P_{cond.}$	36.7
			$P_{sw.}$	29.4
	Inductor (L3, L4)	Chang-sung CH572060E (Toroid)	P_{core}	1.65
			P_{copper}	0.007
	Capacitor (C3, C4)	Digital Tech (250V, 15uF, ESR 0.04Ω)	P_{ESR}	69.2
Total Loss			284.12	

APPENDIX B

TABLE VII
COST ESTIMATION BASED ON COST SPREADSHEET PROVIDED IN THE COMPETITION (SCHEME I)

2003 FUTURE ENERGY CHALLENGE

UNIVERSITY: Seoul National University of Technology
NAME OF MAIN CONTACT:
PROJECT NAME: A 10kW Fuel Cell Inverter System
DATE: 17-May

DEVICE	QTY	DESIG	UNIT	MEASURE	VOLT (Vpk)	VOLT (Vrms)	CUR (Avg)	CUR (Arms)	UNIT COST	EXTENDED COST
DIODE	1	D1			57.6		266.3		3.45	3.45
DIODE	4	D2~D5			410		13.75		2.57	10.29
IGBT	4	S6~S9			420		28		4.77	19.06
MOSFET	1	S1			57.6		214.4		10.45	10.45
MOSFET	4	S2~S5			57.6		353.51		14.76	59.06
CAP (ALUM)	1	C1	3300	uF	77.7				2.86	2.86
CAP (ALUM)	2	C2, C3	5000	uF	210				30.63	61.26
CAP (ALUM)	2	C4, C5	15	uF	170				0.16	0.32
CHOKE	1	L1	50	UH				272.5	251.27	251.27
CHOKE	2	L2, L3	100	UH				24.1	43.79	87.59
CHOKE	2	L4, L5	123	UH				42	52.81	105.63
TRANSFORMER	1	T1				46.4		381.3	25.75	25.75
TRANSFORMER										
CONTROL										
TOTAL										636.98

TABLE VIII
COST ESTIMATION BASED ON COST SPREADSHEET PROVIDED IN THE COMPETITION (SCHEME II)

2003 FUTURE ENERGY CHALLENGE

UNIVERSITY: Seoul National University of Technology
NAME OF MAIN CONTACT:
PROJECT NAME: A 10kW Fuel Cell Inverter System
DATE: 17-May

DEVICE	QTY	DESIG	UNIT	MEASURE	VOLT (Vpk)	VOLT (Vrms)	CUR (Avg)	CUR (Arms)	UNIT COST	EXTENDED COST
DIODE	8	D1~D8			410		6.25		2.29	18.34
IGBT	4	S5~S8			420		28		4.77	19.06
IGBT	4	S11~14			420		9.5		1.69	6.77
MOSFET	4	S1~S4			41		125		6.56	26.24
MOSFET	2	S9, S10			140		62		8.47	16.95
CAP (ALUM)	2	C1, C2	3222	uF	210				19.78	39.55
CAP (ALUM)	2	C3, C4	16	uF	170				0.17	0.33
CHOKE	2	L1, L2	100	UH				14.7	41.72	83.44
CHOKE	2	L3, L4	93	UH				63.1	61.52	123.03
CHOKE	1	L5	40	UH				121.4	73.96	73.96
TRANSFORMER	2	T1				47.3		194.9	16.42	32.84
TRANSFORMER	1	T2				58		78.8	11.30	11.30
CONTROL										
TOTAL										451.82

REFERENCES

[1] R. Anahara, S. Yokokawa, and M. Sakurai, "Present status and future prospects for fuel cell power systems," in *Proc. IEEE*, vol. 81, no. 3, Mar. 1993, pp. 399–407.

[2] M. W. Ellis, M. R. Von Spakovsky, and D. J. Nelson, "Fuel cell systems: Efficient, flexible energy conversion for the 21st century," *Proc. IEEE*, vol. 39, no. 12, pp. 1808–1818, Dec. 2001.

[3] N. Azli and A. Yatim, "DSP-based Online Optimal PWM Multilevel Control for Fuel Cell Power Conditioning Systems," in *Proc. IEEE IECON'01*, vol. 2, 2001, pp. 921–926.

[4] R. Gopinath, D. Kim, J. H. Hahn, M. Webster, J. Burghardt, S. Campbell, D. Becker, P. N. Enjeti, M. Yeary, and J. Howze, "Development of a low cost fuel cell inverter system with DSP control," in *Proc. IEEE PESC'02*, vol. 1, Jun. 2002, p. 309–314.

[5] A. H. Anbuk y and P. E. Pascoe, "VRLA battery state-of-charge estimation in telecommunication power systems," *IEEE Trans. Ind. Electron.*, vol. 47, no. 3, pp. 565–573, 2000.

[6] X. Wang and T. Stuart, "Charge measurement circuit for electric vehicle batteries," *IEEE Trans. Aerosp. Electron. Syst.*, vol. 38, no. 4, pp. 1201–1209, 2002.

[7] K. Wang, C. Y. Lin, L. Zhu, D. Qu, F. C. Lee, and J. S. Lai, "Bi-directional DC to DC converters for fuel cell systems," in *Proc. Conf. Rec. IEEE Workshop on Power Electronics in Transportation*, 1998, pp. 47–51.

[8] The 2003 International Future Energy Challenge Web Site [Online]. Available: http://www.energychallenge.org/

[9] Texas Instruments [Online]. Available: http://www.ti.com/

[10] Design Application Note.MAGNETICS. INC.

[11] A. I. Pressman, *Switching Power Supply Design*. New York: McGraw-Hill, 1999.

[12] J. Lee, J. Jo, S. Choi, and S. Han, "A 10 kW SOFC-low voltage battery hybrid power processing unit for residential use," in *Proc. Fuel Cell Seminar*, Nov. 2003, pp. 33–40.

Jinhee Lee was born in Seoul, Korea, in 1976. He received the B.S. and M.S. degrees from the Department of Control and Instrumentation Engineering from Seoul National University of Technology, Seoul, Korea, in 2003 and 2005, respectively.

He is currently an engineer of The Research and Development Center, Hyosung Heavy Industries, Seoul, Korea. His research interests include power conditioning system for fuel cells, power converter design for hybrid electrical vehicle, and advanced power converter topologies.

Mr. Lee received a Grand Prize Award from the 2003 International Future Energy Challenge sponsored by the U.S Department of Energy.

Jinsang Jo was born in Cheongyang, Korea, in 1977. He received the B.S. and M.S. degrees from the Department of Control and Instrumentation Engineering, Seoul National University of Technology, Seoul, Korea, in 2003 and 2005, respectively.

His research interests include power conditioning system for fuel cells, bidirectional dc-dc converter design for hybrid electrical vehicles and fuel cell vehicles, and magnetic design.

Mr. Jo received a Grand Prize Award from the 2003 International Future Energy Challenge sponsored by the U.S Department of Energy.

Sewan Choi (S'92–M'96–SM'04) received the B.S. degree in electronic engineering from Inha University, Incheon, Korea, in 1985 and the M.S. and Ph.D. degrees in electrical engineering from Texas A&M University, College Station, in 1992 and 1995, respectively.

From 1985 to 1990, he was with Daewoo Heavy Industries as a Research Engineer. From 1996 to 1997, he was a Principal Research Engineer at Samsung Electro-Mechanics Company, Korea. In 1997, he joined the Department of Control and Instrumentation Engineering, Seoul National University of Technology, Seoul, Korea, where he is currently an Associate Professor. His research interests include utility interface and power quality issues including three-phase power factor correction and power conversion technologies in renewable energy systems.

Dr. Choi directed a student team to design and build a 10-kW fuel-cell inverter for residential applications, which won the 1st place award in the 2003 Future Energy Challenge Competition sponsored by U.S. Department of Energy.

Soo-Bin Han (M'95) was born in Korea on June 9, 1958. He received the B.S. degree in electronic engineering from Hanyang University, Korea, in 1981 and the M.S. and Ph.D. degrees in electrical engineering from the Korea Advanced Institute of Science and Technology (KAIST) in 1986 and 1997, respectively.

He has been a Principal Researcher at the Korea Institute of Energy Research (KIER), Daejeon, Korea, since 1986 and now a Leader of the Electric Energy and Lighting Research Center. His research interests include electric energy saving/storage technology, hydrogen/fuel-cell power application, and new lighting technology.